STRUCTURE AND INFRASTRUCTURE ENGINEERING
https://doi.org/10.1080/15732479.2025.2461635

Uncertainty quantification of structural displacement based on multi-response surfaces method for a long-span concrete cable-stayed bridge with damages

Youbao Jiang[a], Zupan Zhang[a], Jing Cai[a], Yu Leng[a], Sondipon Adhikari[b] and Zhibin He[a]

[a]School of Civil Engineering, Changsha University of Science and Technology, Changsha, China; [b]James Watt School of Engineering, Glasgow Univ, Glasgow, UK

ABSTRACT

For long-span cable-stayed bridges, the unpredictable damages and complex structure result in significant challenges of solving displacement and quantifying the uncertainty of structural displacement. An effective approach to solve structural displacement and quantify its uncertainty is proposed based on the multiple response surfaces method. Taking a long-span cable-stayed bridge in China as an example, the main steps are illustrated. First, the damage modes of the materials, members, and structures are determined to establish the corresponding damage uncertainty analysis models. Depending on the combinations of different damaged members, 13 typical damaged conditions are selected for the structural damage mode. After that, a surrogate model for solving the structural displacement is built based on the multi-response surfaces method and uncertainty parameters of damaged materials and other factors. Subsequently, the displacement under corresponding damage conditions is calculated, the uncertainty of the structural displacement is quantified with MCS and Sobol method. Numerical results showed that the variation coefficient of the structural displacement is about twice that of the damaged material elastic modulus, and the damages do have a larger influence on the variation of displacement. Additionally, the proposed method can solve the structural displacement efficiently and be well applied to the long-span structures.

ARTICLE HISTORY
Received 2 April 2024
Revised 3 October 2024
Accepted 4 October 2024

KEYWORDS
Multi-response surfaces; damage uncertainty; surrogate model; Monte Carlo simulation; Sobol method; long-span bridge; structural displacement

1. Introduction

Long-span cable-stayed bridges are widely used in coastal areas; therefore, they are possibly subjected to damages caused by the corrosion of Cl^-, SO_4^{2-}, and CO_2 in the environment (Al-Mosawe, Neves, & Owen, 2022; Meda, Mostosi, Rinaldi, & Riva, 2014). Resultantly, the structural performance degrades over time while the structural displacement increases. Furthermore, the damage uncertainties usually have an influence on the structural displacement. To accurately evaluate the structural displacement during service lifetime, it is important to quantify the influence of damage uncertainty on the long-span cable-stayed bridges. Besides, the uncertainty quantification provides a foundation for implementing reliability-based optimization design (Jiang, Zhang, Beer, Zhou, & Leng, 2024) and improving long-term structural performance.

In engineering practice, the evolution process of structural failure can usually be considered as an accumulation of damage. The accumulation of material damage leads to the damage of members, and a certain degree of accumulation of member damage leads to structural failure. Thus, material damage is the primary link to structural damage.

At the beginning of the studies, evolution equations of material performance were proposed (Kachanov, 1999; Rabotnov, 1963), and the damage variable D was initially introduced to describe the change in performance state caused by material damage. Next, Lemaitre (1971) innovated damage mechanics in different fields, e.g. ductile damage and low cycle fatigue damage. Then, several concrete damage models (Lu, Meng, Zhou, Wang, & Du, 2022; Wang, 2023; Wang & Li, 2022; Zhang, Lu, & Cao, 2020) and steel fracture damage models (Chen, Zhang, Chen, Li, & Xing, 2023; Margolin, Fomenko, Shvetsova, & Yurchenko, 2022; Shang, Yang, Su, & Wang, 2023; Shen & Wu, 2007) were established by considering various stress conditions and material types. With the aforementioned material damage models, it is possible to obtain the time-varying laws of strength, stress-strain relationship, and fatigue life, respectively, and the elastic modulus of a material is a critical parameter in these time-varying laws. Thus, the method of reducing the elastic modulus can be selected to study the damage mode of the material.

Moreover, the effects of damages were reported for the cable-stayed bridges, e.g. the effect of tension damages in single-cable and multi-cables systems on the stress loss of cables (Nazarian, Ansari, Zhang, & Taylor, 2016), the effects of member damages on the static performance of cable-stayed bridges (Ma, Peng, Lei, & Zhang, 2022), the effects of cable ruptures on the cracking behavior of the main girder (Zhang, Fang, et al., 2020), and the effects of cable ruptures on the impact resistance ability of bridges (Hoang, Kiyomiya, & An, 2018). It

CONTACT Yu Leng lengyu@csust.edu.cn School of Civil Engineering, Changsha University of Science and Technology, Changsha 410114, China.
Supplemental data for this article can be accessed online at https://doi.org/10.1080/15732479.2025.2461635.

is well known that long-span cable-stayed bridges have complex force transmission paths and many uncertain factors (e.g. stress conditions, damage conditions, and environmental conditions). Thus, the structural performance function is generally implicit and nonlinear.

On this condition, the Monte Carlo simulation (MCS) and response surface methodology (RSM) were employed to quantify the uncertainty of structural response in earlier studies. However, the fitting efficiency of the conventional RSM is usually low, and the fitting equation is inaccurate, too. Then, the iterative approach and Support Vector Machine (SVM) were integrated with the RSM to enhance the accuracy and efficiency of the function fitting. Due to the curse of dimensionality, these methods (Hadidi, Azar, & Rafiee, 2017; Ju, Shenoi, Jiang, & Sobey, 2013; Ren, Fang, & Deng, 2011) still cannot be well applicable for large complex structures with high-dimensional implicit failure equations. Therefore, the multi-response surfaces (MRS) method is proposed to reconstruct the high-dimensional explicit performance function of complex structural systems (Jiang, Huang, Liao, & Zhang, 2015a, Jiang, Luo, Liao, Zhao, & Zhang, 2015b).

In addition, it has been found that the structural performance function has a better fitting effect, and the MRS method is suitable for long-span structures with high-dimensional failure equations (Jiang et al., 2017; Jiang, Zhao, Beer, Wang, & Zhang, 2020; Jiang et al., 2021). Herein, the structural displacement of a long-span concrete cable-stayed bridge with damage can be solved based on the MRS method, and the uncertainty analysis of structural displacement can be performed. To simplify the analysis, the static effects of bridge structure under the basic load combination are considered, and the dynamic effects caused by autocorrelation of the loads are neglected, as reported by Truong & Kim (2017) and Zhang, Li, Ding, & Wu (2020).

The main sections of this study are illustrated. First, the elastic modulus of the material and the stiffness of the main girder cross-section are selected as the damage indicators for the material and the member, respectively. The structural damage mode is considered by combining different damaged members. Then, a surrogate model for solving the structural displacement is built based on the multi-response surfaces method. Finally, the uncertainty of structural displacement is quantified with MCS, and the corresponding sensitivity analysis is conducted.

2. Damage mode of long-span concrete cable-stayed bridges

In this paper, the damage modes of material, member, and structure are considered for the long-span concrete cable-stayed bridge. The details are provided in the following.

2.1. Damage mode of material elastic modulus

The nominal elastic modulus of the material is selected as the damage index to establish the uncertainty analysis model. Moreover, the time factor is a critical parameter in this model because the mechanical performance of damaged materials often degrades with the increase of service years.

2.1.1. Degradation of the elastic modulus for concrete

According to Lemaitre's principle of strain equivalence, the strain caused by the stress σ acting on the damaged element is equivalent to the strain caused by the effective stress σ_t acting on the undamaged element. Thus, the constitutive relationship of the damaged material can be expressed using the nominal stress of the nondestructive material, and it is given by:

$$\frac{\sigma}{E_t} = \varepsilon = \frac{\sigma_t}{E_0} = \frac{\sigma}{(1 - D(t))E_0} \tag{1}$$

where E_0 is the initial (undamaged) elastic modulus of material; E_t is the actual elastic modulus of damaged material at moment t; D is the damage evolution factor, which is a critical damage parameter for the Damage Plasticity Model (DPM) (Lubliner, Oliver, Oller, & Oñate, 1989). Based on DPM, several damage factor models were established by considering different force states and engineering characteristics, e.g. considering the effects of cracking (Mourlas, Markou, & Papadrakakis, 2019), considering the effects of uniaxial stress (Bian, Liu, Guo, Liu, & Shi, 2023), considering the effects of underwater environment (Wang et al., 2023).

However, the influence of time factor on D is not considered in these damage factor models. Herein, the damage factor model of concrete proposed by Zheng and Wang (2018) is selected, and $D(t)$ (i.e. the amount of damage factor at moment t) is calculated as:

$$\begin{aligned} D(t) = {} & 4.13 \times 10^{12} \exp\left[-\left(\frac{t - 189.7}{6.684}\right)^2\right] \\ & + 0.6599 \exp\left[-\left(\frac{t - 179}{33.89}\right)^2\right] \\ & - 0.01029 \exp\left[-\left(\frac{t - 189.7}{6.684}\right)^2\right] \\ & - 0.5366 \exp\left[-\left(\frac{t - 586.1}{280.8}\right)^2\right] \\ & + 0.3169 \exp\left[-\left(\frac{t - 140.4}{84.51}\right)^2\right] \end{aligned} \tag{2}$$

where t is the service time of the bridge. Then, the time-varying function of the nominal elastic modulus of concrete is obtained based on Equations (1) and (2), and it is given by:

$$\begin{aligned} E_C(t) = E_t &= (1 - D(t))E_0 \\ &= \left\{ \begin{array}{l} 1 - 4.13 \times 10^{12} \exp\left[-\left(\frac{t-189.7}{6.684}\right)^2\right] \\ -0.6599 \exp\left[-\left(\frac{t-179}{33.89}\right)^2\right] \\ +0.01029 \exp\left[-\left(\frac{t-189.7}{6.684}\right)^2\right] \\ +0.5366 \exp\left[-\left(\frac{t-586.1}{280.8}\right)^2\right] \\ -0.3169 \exp\left[-\left(\frac{t-140.4}{84.51}\right)^2\right] \end{array} \right\} \times E_0 \end{aligned} \tag{3}$$

2.1.2. Degradation of the elastic modulus for cable

The cable is composed of steel strands, the elastic modulus reduction model is usually established by calculating the corrosion rate of the steel strands, e.g. the mass loss after chloride penetration (Yu, Gu, Zeng, & Zhang, 2022), the loss of cross-sectional area (Campione & Zizzo, 2022), and the relationship between area loss and mass loss (Lu, Zhou, Li, & Zhao, 2021). However, each degradation model has its specific assumptions and scope of application. Due to the geographical environment and the time factor, the models (Wang, Zhang, Wang, & Zhang, 2015; Yan et al., 2023) shown in Equations (4) - (6) are selected.

The degradation model of elastic modulus after the cable corrosion (Yan et al., 2023) is given by:

$$\frac{E_S}{E_{S0}} = -0.04635\eta + 1 \tag{4}$$

where E_{S0} and E_S are the nominal elastic modulus (MPa) of the cables before and after the corrosions, respectively; η is the corrosion rate, which is given by:

$$\eta = \frac{3}{7}\left[1 - \left(\frac{\Delta r(t)}{r}\right)^2\right] \tag{5}$$

$$\Delta r(t) = 0.116 i_{cor}(t - t_s) \tag{6}$$

where t_s is the beginning time of corrosion (years); i_{cor} is the corrosion current density, and takes the medium corrosion current density 0.25 μA/cm^2 reported by Wang et al. (2015); $\Delta r(t)$ is the radius reduction of the steel wire at moment t; r is the radius of steel wire. Then, with Equations (4)–(6), the time-varying function of the elastic modulus of cable is given by:

$$E_S(t) = E_{S0} \cdot \left\{-0.04635\left[\frac{3}{7}\left(1 - \left(\frac{0.116 i_{cor}(t - t_s)}{r}\right)^2\right)\right] + 1\right\} \tag{7}$$

2.2. Damage mode for sections of members

The bending stiffness of the damaged main girder section is selected as the damage index for the member sections, and it degrades over service time. It is assumed that the main girder is a constant section girder, the configuration of the half cross-section of this girder is given in Figure 1a. Besides, it is considered that the variability mainly comes from the corrosion of the concrete cover of the main girder, resulting from the contact with the sea.

For this simplified case, two assumptions are adopted for the damage analysis: (1) the whole cross-section of the main girder is divided into a damaged zone (S_2 zone) and an undamaged zone (S_1 zone) as shown in Figure 1a; (2) the degree of damage is not large, and the stress of the cross-section conforms to the plane section assumption (as seen in Figure 1b). In the following calculations, the damaged concrete zones are assumed to be located in the bottom slabs and webs of the main girder, as the zones marked with oblique lines in Figure 1a.

Let d denote the damage depth, as shown in Figure 1a. It is well known that d can be affected by many factors, e.g. time, stress state, humidity, and CO_2 concentration. Several models were established considering different environmental factors and stress states (Elsalamawy, Mohamed, & Kamal, 2019; Londhe et al., 2021; Paul, Panda, Huang, Garg, & Peng, 2018). Due to the flexural loads and environmental characteristics, the model reported by Liu et al. (2023) is selected to calculate d, and it is given by:

$$d = f(\mathrm{RH}) \cdot f(\sigma) \cdot k_{C0} \cdot \sqrt{0.2t} \tag{8}$$

where f (RH) is the RH (relative humidity) influence coefficient, and takes 1.19 reported by Liu et al. (2023); $f(\sigma)$ is the flexural load influence coefficient, and it can be acquired from Liu et al. (2023); k_{C0} is the concrete carbonation coefficient when σ is 0, and takes 2.94 reported by Liu et al. (2023).

Suppose z denotes the vertical coordinate, z_0 denotes the neutral axis coordinate of the whole section. The points B_1 and B_2 are assumed to be the centroids of the undamaged and damaged zones, respectively. According to the plane section assumption, the strain diagram is given in Figure 1b. Next, the stress-strain relationships of undamaged and damaged concrete are calculated as Equation (9) and Equation (10), respectively, based on the strain diagram and Hooke's law. Additionally, the static equilibrium condition for the normal section of the main girder is calculated as Equation (11):

$$\sigma_1 = E_1 \cdot \varepsilon_1 = E_1 \cdot \frac{z_1 - z_0}{a - z_0} \cdot \varepsilon_{\max} \tag{9}$$

$$\sigma_2 = E_2 \cdot \varepsilon_2 = E_2 \cdot \frac{z_2 - z_0}{a - z_0} \cdot \varepsilon_{\max} \tag{10}$$

$$\int_{S_1+S_2} \sigma \mathrm{d}S = \int_{S_1} \sigma_1 \mathrm{d}S + \int_{S_2} \sigma_2 \mathrm{d}S = 0 \tag{11}$$

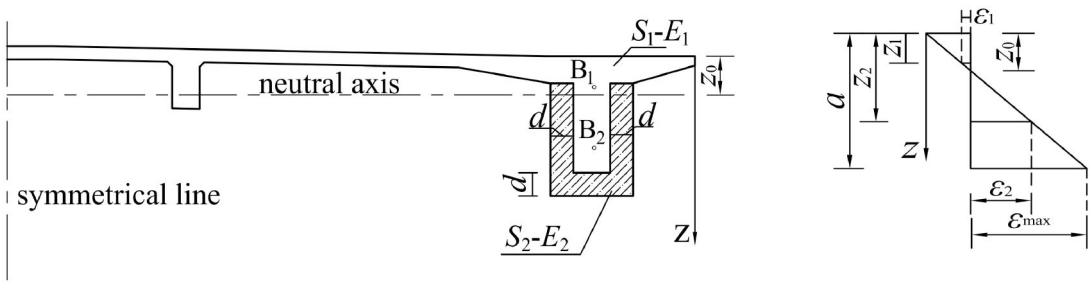

Figure 1. Diagram for the girder: (a) configurations of the half cross-section; (b) strain relationship.

where E_1 and E_2 are the elastic modulus of the undamaged and damaged concrete, respectively; ε_1 and ε_2 are the strain of the undamaged and damaged zone, respectively; ε_{max} is the maximum strain of cross-section of the main girder; a is the height of cross-section of the main girder, and takes 3 m for this example; z_1 and z_2 are the vertical coordinates of B_1 and B_2, respectively; S_1 and S_2 are the area of the undamaged and damaged zone, respectively.

Subsequently, the bending stiffness K of the compound section is calculated as:

$$K = E_1 I_{1z0} + E_2 I_{2z0} = E_1 \int_{S_1} (z - z_0)^2 \mathrm{d}S + E_2 \int_{S_2} (z - z_0)^2 \mathrm{d}S \tag{12}$$

where I_{1z0} and I_{2z0} are the moment of inertia of the undamaged and damaged zone about the neutral axis; the neutral axis coordinate z_0 of the whole cross-section can be determined by solving Equations (9)–(11). It is usually difficult to directly simulate the damage to the main girder using stiffness K in the subsequent calculation of structural displacement. However, the variation of the stiffness K of the girder section can be reflected by the elastic modulus. Therefore, an equivalent elastic modulus E' of the damaged girder section (Equation (13)) is defined according to the principle of equivalent bending stiffness, and it is used for the simulation of the damage to the main girders:

$$E' = \frac{E_1 \int_{S_1} (z - z_0)^2 \mathrm{d}S + E_2 \int_{S_2} (z - z_0)^2 \mathrm{d}S}{\int_{S_1 + S_2} (z - z_0)^2 \mathrm{d}S} \tag{13}$$

2.3. Damage mode for structure

For a long-span concrete cable-stayed bridge, the mid-span deflection and bending moment of its main span are usually selected to evaluate the structural response. As mentioned in Section 2.1 and Section 2.2, the structural response can be influenced by the damaged materials and member sections. Besides, the structural response of a cable-stayed bridge is also influenced by load variations and the various potential combinations of damage locations of the main girder and cables.

It is well-known that the structural response at a specific position can be accurately evaluated by the influence line, when the unit load acts on different positions of the girder. Herein, the influence line analysis can be employed to identify the most unfavorable load locations, and the girder segments at those corresponding positions are mainly considered for making combinations. For the common long-span symmetrical double tower cable-stayed bridges, the simplified schematic diagram of the bridge is shown in Figure 2, where the auxiliary piers are usually used to reduce the deflection deformation of the side span and improve the stiffness of the main span. The damage locations of this cable-stayed bridge are determined as follows.

First, for the cables, it is reported by Wei and Pan (2020) that the outermost damaged cable has a greater influence on the structural response. Therefore, the outermost cable of each span is mainly considered for the calculation of the mid-span deflection of the bridge. In the case of the symmetrical double tower cable-stayed bridge shown in Figure 2, the outermost cables of each span, (named C1, C2, C3, and C4) are selected to study the influence of damaged cables on the structural response.

Secondly, for the main girder with a uniform section, the influence line analysis is used to identify the unfavorable load locations. Let the unit load move along the span direction of the bridge. The relationships between the structural response and the position of the unit load can be acquired by mechanical analysis, e.g. the dashed lines shown in Figure 2 are the influence lines. Moreover, the value of the influence line represents the response of the physical quantities (e.g. mid-span bending moment and mid-span deflection).

Herein, the position corresponding to the maximum value of the influence line can be selected as the most unfavorable damage location. For instance, based on the influence line of the mid-span deflection (Figure 2a) and the influence line of the mid-span bending moment (Figure 2b), Point 1, Point 2, and Point 3 are selected as the damaged locations. Finally, based on the principle that both the girder segments and the cables are damaged, different damaged girder segments and cables are combined to get various damage conditions.

3. Displacement solving for cable-stayed bridge with multi-response surfaces method

3.1. Multi-response surfaces method for limit state equation fitting

It is well known that the displacement is usually influenced by many uncertain factors (e.g. elastic modulus of cables, elastic modulus of concrete, and loads) for a long-span cable-stayed bridge. To quantify the uncertainty of structural displacement, the Monte Carlo sampling is usually used. In this case, an efficient model rather than the finite element model is needed for solving the displacement. Herein, an explicit equation about the displacement is fitted with the MRS method firstly, where the sample pairs and SVM techniques are used to fit the equation. The specific steps are as follows:

3.1.1. Generation of initial sample pairs in real space

To use SVM techniques for function fittings, the uniform design method is employed to produce initial sample pairs, and then the sample pairs can be distributed uniformly over the design space. Herein, if n random variables are given, a uniform design table U_h (q^n) is selected to determine the initial sample points $\boldsymbol{x}$ in the standard normal space, where h, q, and n are table parameters (see Jiang et al., 2017); the element u_{ij} in the table can be mapped to the actual range of values of the variables by linear mapping (see Fang, Lin, Winker, & Zhang, 2000). Generally, the sampling range of variable in the standard normal space is assumed as $[-\lambda, \lambda]$.

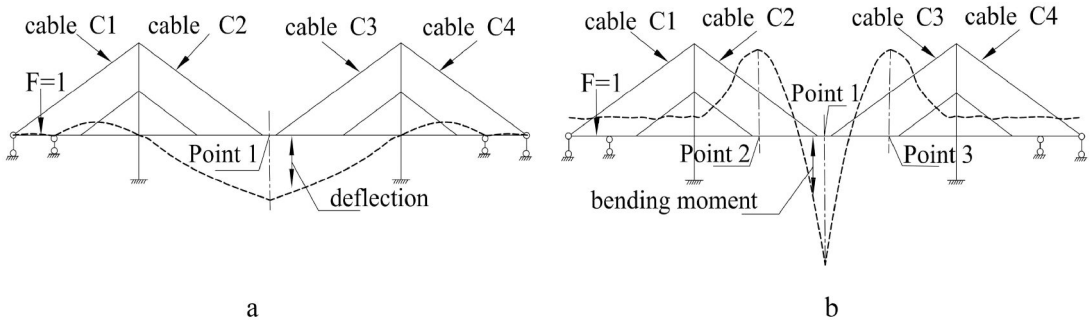

Figure 2. Influence lines of the bridge: (a) the mid-span deflection; (b) the mid-span bending moment.

Thus, the ith sample value of the jth variable x_j in the standard normal space is given by a simplified equation:

$$x_{ij} = \left[\frac{2(u_{ij}-1)}{q-1} - 1\right]\lambda \quad (i = 1, 2, \ldots, h;\ j = 1, 2, \ldots, n) \tag{14}$$

where u_{ij} is usually an integer in [1, q] and means a certain level of the jth variable at the ith experiment design; λ is a range parameter and usually taken 3 (Jiang, Luo, Liao, Zhao, & Zhang, 2015b).

Next, let $\boldsymbol{x} = (x_1, x_2, \ldots, x_n)$ denote the sample point in the standard normal space. Then, the h uniform sample points in the standard normal space are transformed into those in the real space with Equation (15) for the structural failure analysis:

$$y_{ij} = \mathrm{F}_{j,\mathrm{cd}}^{-1}\left[\Phi(x_{ij})\right] \tag{15}$$

where $\Phi(\cdot)$ is the cumulative distribution function (CDF) of the standard normal variable x_j; $\mathrm{F}_{j,\mathrm{cd}}^{-1}(\cdot)$ is the corresponding inverse function of variable y_j with CDF $\mathrm{F}_{j,\mathrm{cd}}(\cdot)$.

Generally, the variables of structures are divided into two parts: resistance variables and load variables. Let $\boldsymbol{R}$ denote the resistance vector, $\boldsymbol{S}$ denote the load vector, the sample point can be expressed by SP = ($\boldsymbol{R}$, $\boldsymbol{S}$). For a sample point $\boldsymbol{y} = [y_1, \ldots, y_{n_1}, y_{n+1}, \ldots, y_n]$ obtained from Equation (15), there are n variables in sample point $\boldsymbol{y}$, where $y_1, y_2, \ldots, y_{n_1}$ are n_1 resistance variables; $y_{n_1+1}, y_{n_1+2}, \ldots, y_{n_1+n_2}$ are n_2 load variables; $n_1 + n_2 = n$. Next, let $\boldsymbol{r} = \left[1, y_{n_1+2}/y_{n_1+1}, \ldots, y_{n_1+n_2}/y_{n_1+1}\right]$ denote the load ratio vector, the load variables vector can be expressed by $\boldsymbol{S} = y_{n_1+1}\boldsymbol{r}$.

Then, according to Jiang et al. (2017), the initial sample pairs SP_1 and SP_2 in the safe domain and failure domain, respectively, can be acquired by:

$$\mathrm{SP}_1 = \left\{y_1, y_2, \ldots, y_{n_1}, F_s\left[1, \frac{y_{n_1+2}}{y_{n_1+1}}, \ldots, \frac{y_{n_1+n_2}}{y_{n_1+1}}\right]\right\} \tag{16}$$

$$\mathrm{SP}_2 = \left\{y_1, y_2, \ldots, y_{n_1}, F_f\left[1, \frac{y_{n_1+2}}{y_{n_1+1}}, \ldots, \frac{y_{n_1+n_2}}{y_{n_1+1}}\right]\right\} \tag{17}$$

where F_s and F_f are safe load factor and failure load factor, respectively, corresponding to a serviceability limit state. They can be calculated as: $F_s = (1\text{-}\ \varepsilon)\ S_{\mathrm{lim}}$ and $F_f = (1+\ \varepsilon)\ S_{\mathrm{lim}}$, where ε is a precision control factor and generally taken as 0.05; S_{lim} is the limit load factor corresponding to the load variable y_{n_1+1} in point $\boldsymbol{y}$, and it is calculated as Equation (18) because the load is proportional to the structural displacement with linear elastic force under the normal use condition:

$$\frac{\Delta_{S\mathrm{lim}}}{\Delta_{S0}} = \frac{S_{\mathrm{lim}}}{S_0} \tag{18}$$

where S_0 is the initial load factor corresponding to the load variable y_{n_1+1} in the initial sample point $\boldsymbol{y}$; Δ_{S0} is the displacement corresponding to the initial sample point, and it is usually calculated by the deterministic structural failure analysis; Δs_{lim} is the displacement corresponding to a serviceability limit state (e.g. l/500 for the following analysis, and l is the length of the main span of bridges).

Taking two basic variables R (resistance variable) and S (load variable) as an example, as shown in Figure 3. Suppose there is a sample point P_0 (R_0, S_0), the corresponding limit state sample point P_0 (R_0, S_{lim}) is generated with the fixed resistance variable R_0 and linear Equation (18). Then, the corresponding sample pairs corresponding to a serviceability limit state can be generated with Equations (16) and (17).

3.1.2. Subspace division based on initial sample pairs in standard normal space

The SVM techniques cannot be directly used for response surface fitting because the dimensions of variables in real space are different. To unify dimensions, the limit state sample pairs in real space are transformed into those in standard normal space with:

$$x_j = \Phi^{-1}\left[\mathrm{F}_{j,\mathrm{cd}}(y_j)\right] \qquad (j = 1,\ 2,\ \ldots,\ n) \tag{19}$$

where $\mathrm{F}_{j,\mathrm{cd}}(\cdot)$ is the cumulative distribution function (CDF) of variable y_j; $\Phi^{-1}(\cdot)$ is the corresponding inverse function of the standard normal variable x_j.

It is reported by Jiang et al. (2017) that the closer the point on limit state surface is to the origin in the normal standard space, the more that contributes to the failure probability. Thus, the distance from any sample point to the origin in standard normal space is calculated to find $\boldsymbol{x}_0$ which is the closest sample point to the origin. With Equation (20), an inner product coefficient $\rho_0(i)$ of $\boldsymbol{x}_0$ and $\boldsymbol{x}_i$ is calculated. And the total space is divided into multiple subspaces by the values of $\rho_0(i)$ (i is the number of sample points):

$$\rho_0(i) = (\boldsymbol{x}_0 \cdot \boldsymbol{x}_i)/\|\boldsymbol{x}_0\|/\|\boldsymbol{x}_i\| \tag{20}$$

First, sort the values of $\rho_0(i)$ for all sample points with Equation (21). Next, according to the principle that the number of sample points in each subspace is twice the number of variables (Jiang et al., 2017), the number of subspaces

is obtained. If s is assumed to be the number of subspaces, the subspace ranges are [ρ_0 (m), ρ_0 (m-1)] ($m = 1, 2, \ldots, s$), where $\rho_0(m)$ is obtained by Equation (22) and satisfies Equation (21):

$$1 = \rho_0(1) \geq \rho_0(2) \geq \cdots \geq \rho_0(i) \tag{21}$$

$$\rho_0(m) = \left[\rho_0\left(\sum_{i=1}^{m} n_i\right) + \rho_0\left(\sum_{i=1}^{m} n_i + 1\right)\right]/2 \tag{22}$$

where n_i is the number of sample points in the i-th subspace.

3.1.3. Fittings of limit state equation with iterative correction

With SVM techniques (Jiang et al., 2017), the limit state equation in the standard normal space is fitted separately by Equation (23) for each subspace, and the sample point pairs can be classified correctly, as shown in Figure 4a:

$$(\alpha_1 x_1 + \cdots + \alpha_n x_n) + \left(\alpha_{n+1} x_1^2 + \cdots + \alpha_{2n} x_n^2\right) + b = 0 \tag{23}$$

where b, α_j are fitting coefficients; n is the number of variables.

To accurately fit the limit state equation, more sample pairs are needed. Firstly, the FORM method is employed to solve the design points corresponding to the current limit state equation of each subspace, subsequently, these design points are transformed into those in the real space with Equation (15). Then, execute a structural analysis, the additional sample pairs (ASP) corresponding to the design points are generated with Equations (16)–(19), as shown in Figure 4b. If the ASP can be correctly separated by the current limit state equation, the iteration is ended. Otherwise, add these ASP to update the current set of samples, and go step (2) to update the subspace division. Then the limit state equation is also updated with SVM techniques.

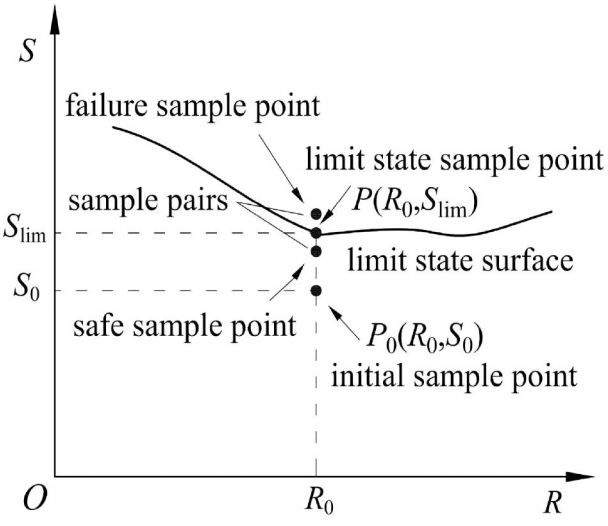

Figure 3. Diagram for generation of sample point pairs (two variables).

3.2. Displacement solving based on the fitted limit state equations

The variables in Equation (23) are dimensionless because this limit state equation (Equation (23)) is constructed in the standard normal space. However, the objective unknown Δ_S (e.g. the mid-span deflection of bridge) is a physical quantity in the real space. Herein, it is necessary to transform the limit state equation into an equation in the real space, and then, a new equation about structural displacement Δ_S in real space is constructed. The specific steps are as follows.

3.2.1. Transformation of the limit state equation

Let Norm $(\cdot)$ denote a function of normalization, then, the Equation (23) in standard normal space is transformed into an equation in real space and it is given by:

$$\begin{aligned}&\alpha_1 \mathrm{Norm}(y_1) + \cdots + \alpha_{n_1} \mathrm{Norm}(y_{n_1}) + \alpha_{n_1+1} \mathrm{Norm}(y_{n_1+1}) \\ &+ \cdots + \alpha_n \mathrm{Norm}(y_n) + \alpha_{n+1} \left[\mathrm{Norm}(y_1)\right]^2 \\ &+ \cdots + \alpha_{n+n_1} \left[\mathrm{Norm}(y_{n_1})\right]^2 + \alpha_{n+n_1+1} \left[\mathrm{Norm}(y_{n_1+1})\right]^2 \\ &+ \cdots + \alpha_{2n} \left[\mathrm{Norm}(y_n)\right]^2 + b = 0\end{aligned} \tag{24}$$

3.2.2. Construction of explicit equation for displacement solving

For a given sample point $\boldsymbol{y} = [y_1, \ldots, y_{n_1}, y'_{n_1+1}, \ldots, y'_n]$, with the fixed resistance variables $y_1, \ldots, y_{n_1}$, let $\boldsymbol{r} = [1, y'_{n_1+2}/y'_{n_1+1}, \ldots, y'_n/y'_{n_1+1}]$ denote the load ratio vector. Next, the limit load factor y_{n_1+1} is acquired as $y_{n_1+1} = (\Delta_{\lim}/\Delta_S) * y'_{n_1+1}$ by taking the initial load factor y'_{n_1+1} into Equation (18). And the corresponding limit load variables $y_{n_1+1}, \ldots, y_n$ satisfying Equation (24) are obtained by $y_{n_1+1}\boldsymbol{r}$. Then, the limit load variables can be replaced with $(\Delta_{\lim}/\Delta_S) * y'_j$ (j=n_1+1, …, n),

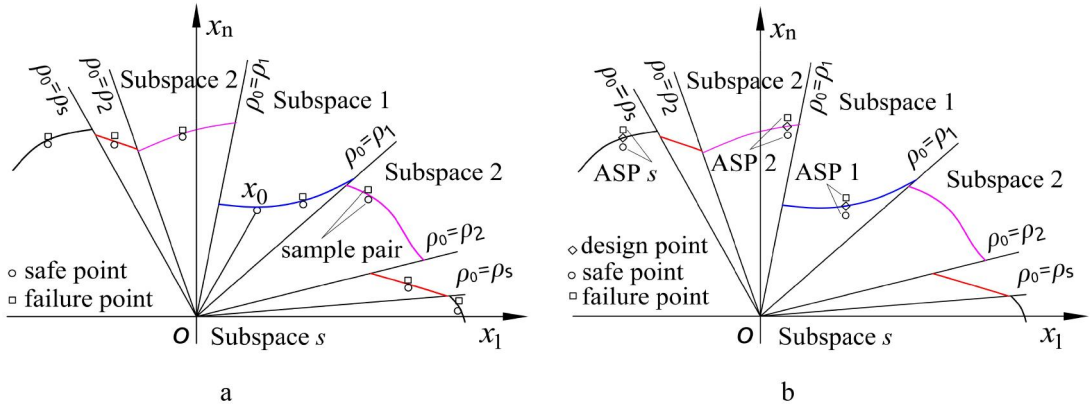

Figure 4. Diagram for the limit state equation fitting: (a) classification of the limit state sample point pairs; (b) generation of the additional sample point pairs.

and the explicit displacement solving equation is given by:

$$\alpha_1 \mathrm{Norm}(y_1) + \cdots + \alpha_{n_1} \mathrm{Norm}(y_{n_1}) + \alpha_{n_1+1} \mathrm{Norm}\left(\frac{\Delta_{\lim} y'_{n_1+1}}{\Delta_S}\right) + \cdots + \alpha_n \mathrm{Norm}\left(\frac{\Delta_{\lim} y'_n}{\Delta_S}\right) + \alpha_{n+1} \left[\mathrm{Norm}(y_1)\right]^2 + \cdots + \alpha_{n+n_1} \left[\mathrm{Norm}(y_{n_1})\right]^2 + \alpha_{n+n_1+1} \left[\mathrm{Norm}\left(\frac{\Delta_{\lim} y'_{n_1+1}}{\Delta_S}\right)\right]^2 + \cdots + \alpha_{2n} \left[\mathrm{Norm}\left(\frac{\Delta_{\lim} y'_n}{\Delta_S}\right)\right]^2 + b = 0 \tag{25}$$

3.2.3. Solution of displacement equation

For a given sample point $\boldsymbol{y}$, at first, it needs to be transformed into the point $\boldsymbol{x}$ in standard normal space with Equation (19). With Equations (20)–(22), the sample point $\boldsymbol{x}$ in the standard normal space can be classified correctly. Then, the given sample point $\boldsymbol{y}$ is taken into the displacement solving equation of the corresponding subspace acquired from step (2), and the value of Δ_S in Equation (25) can be solved with MATLAB software.

4. Uncertainty analysis for long-span cable-stayed bridges with damages

4.1. Background of the cable-stayed bridge

Taking a long-span concrete cable-stayed bridge in China as an example, the details are shown in Figure 5. This bridge is a symmetrical double-tower cable-stayed bridge with a span arrangement of 210 m + 420 m + 210 m. It is mainly composed of three parts: the main girder with concrete, the main tower with concrete, and the cables with steel strands. The cables are arranged in a symmetrical fan-shape with double cable planes, and 34 pairs of stay cables are arranged for each tower.

In order to describe the damage location clearly, as shown in Figure 5a, the girder is assumed to be divided into four segments: Beam A to Beam D according to the arrangements of the cables. The cable elements include CA34 to CA1, CB1 to CB34, CC34 to CC1, and CD1 to CD34. The tower elements include T1 to T6. The girder elements are corresponded to the cable elements, and they are named as BA34 to BA1, BB1 to BB34, BC34 to BC1, and BD1 to BD34. Then, the finite element model of this symmetrical bridge is built by ANSYS software, with the Link10 element for cables and the Beam188 element for towers and the girder skeleton. The details are shown in Figure 6.

4.2. Uncertainty of damaged materials and members

The initial elastic modulus of concrete and steels are selected as random variables for the corresponding uncertainty analysis model, the parameters of these random variables reported by Wang and Tang (2014) are listed in Table 1.

First, run 30000 Monte Carlo samplings with the given parameters by calling the time-varying equation of material elastic modulus Equation (3) and Equation (7) at three

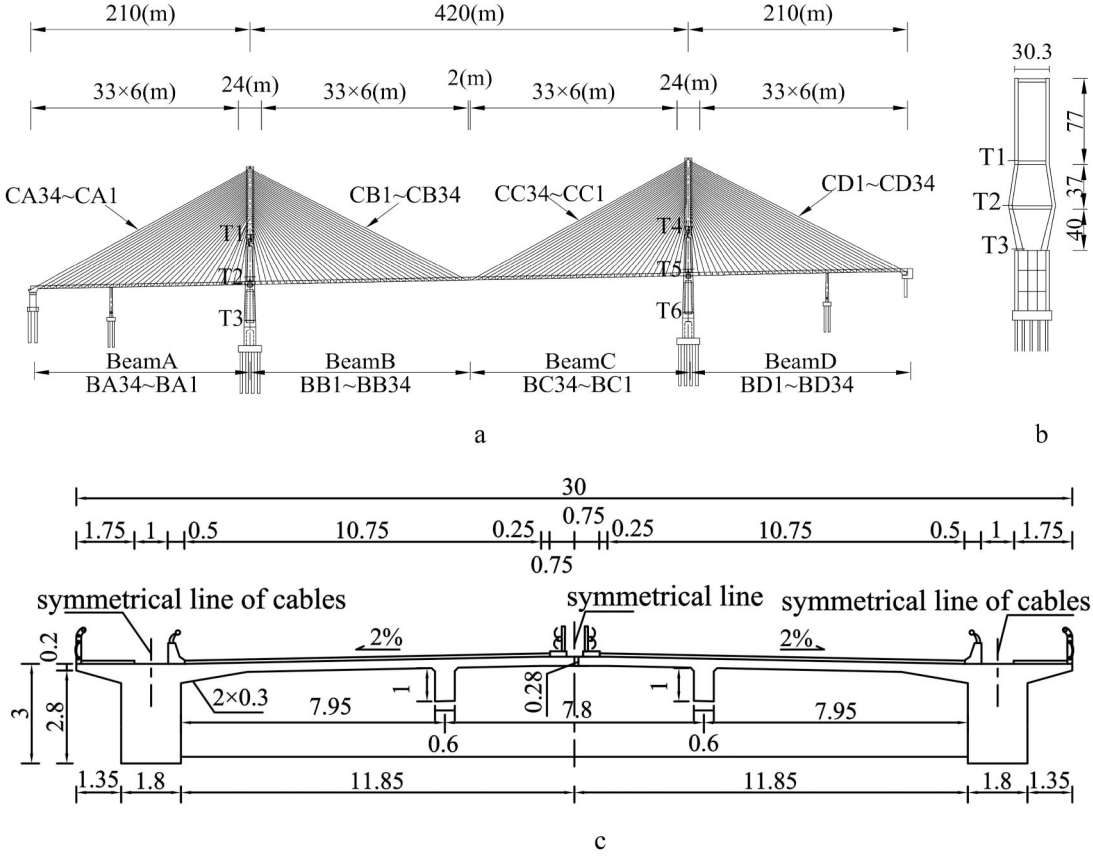

Figure 5. General layout of the bridge (units: m): (a) elevation view; (b) cross-section of bridge tower; (c) cross-section of main girder.

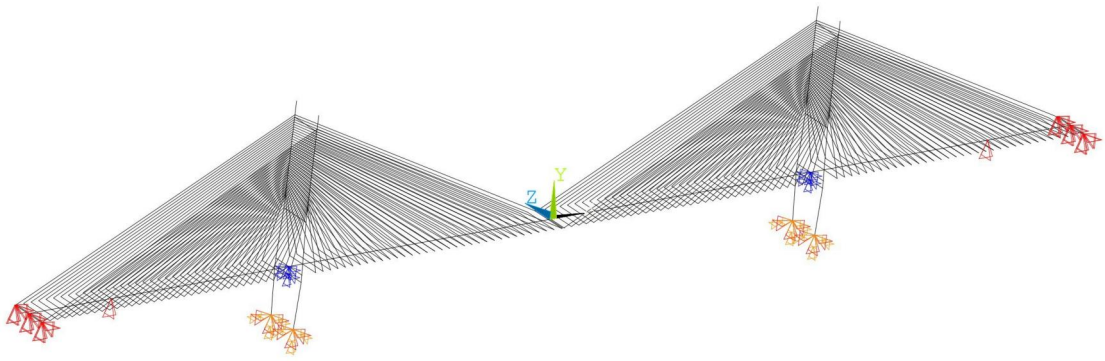

Figure 6. Simplified finite element model of the cable-stayed bridge.

Table 1. Parameters of random variables for the bridge.

No.	Name	Variable	Distribution	Mean μ	Standard deviation σ
1	Elastic modulus of main girder	E_1 / Pa	Normal	3.64×10^{10}	3.64×10^{9}
2	Elastic modulus of cable	E_3 / Pa	Normal	1.95×10^{11}	1.95×10^{10}
3	Volume weight of main girder	γ_1 / N/m^3	Normal	2.66×10^{4}	1.33×10^{3}

Table 2. Damage uncertainty parameters of material and member at different service years.

	Name	Variable	t/a	μ	*cov*	Equation
Material	Elastic modulus of concrete	$E_C(t)$ /Pa	0	3.64×10^{10}	0.100	/
			30	3.32×10^{10}	0.114	Equation (3)
			50	3.13×10^{10}	0.123	Equation (3)
	Elastic modulus of cable	$E_S(t)$ /Pa	0	1.95×10^{11}	0.100	/
			30	1.69×10^{11}	0.119	Equation (7)
			50	1.53×10^{11}	0.129	Equation (7)
Member	Stiffness of the cross-section of the main girder	K /N·m^2	0	9.24×10^{11}	0.103	/
			30	8.08×10^{11}	0.106	Equation (12)
			50	7.84×10^{11}	0.109	Equation (12)

Note: μ denotes the mean value of random variables; σ denotes the standard deviation; *cov* denotes the variation coefficient of random variables. When $t = 0$, the elastic modulus of material takes its own initial elastic modulus

specific moments, respectively. The uncertainty parameters of elastic modulus of the damaged materials can be obtained by the statistics of the sampling results, and they are listed in Table 2.

Next, call the bending stiffness formula (Equation (12)), run 30000 Monte Carlo samplings with the uncertainty parameters of material elastic modulus in Table 2 at three specific moments, respectively. The uncertainty parameters of the stiffness of damaged main girder section can be acquired by the statistics of the sampling results, and the parameters at different service years are listed in Table 2, too. In addition, the corresponding uncertainty parameters can be used for the calculation of structural displacement.

4.3. Uncertainty of structural displacement

4.3.1. Damage condition of cable-stayed bridge

According to the engineering example and the damaged mode for structure, the mid-span position and quarter position of the main span are selected as the damage locations for the main girder. Thus, the girder segments located at the corresponding positions (e.g. key girder Segment1 and Segment2) are selected to study the influence of damaged girders on the deflection. Additionally, the outermost cables of each span (named CA34, CB34, CC34, and CD34) in Figure 7 are selected to study the influence of damaged cables on the deflection. Furthermore, the elastic modulus E' in Equation (13) and E_S in Equation (7) are employed to simulate the damage of the key girder segments and cables, respectively.

With the combination principle proposed in the previous sections, the most unfavorable damage condition DC1 is given. In this condition, all damaged members (i.e. girder segments and cables) are considered. Then, the number of damaged members is gradually reduced to make different combinations. Finally, a total of 13 damage conditions are selected as an attempt to study the influence of structural damage mode on the structural displacement, the details are listed in Table 3.

4.3.2. Selection of random variables

According to the engineering example in earlier sections, it involves 23 variables which describe the various properties of bridge. The variables including the material parameters (e.g. elastic modulus of the outermost damaged cables of each span E_i ($i = 6, 7, 8, 9$), elastic modulus of undamaged cables E_3, elastic modulus of key girder Segment1 and Segment2 (E_4 and E_5), elastic modulus of the undamaged girder segments E_1, elastic modulus of the bridge tower E_2, and the gravity of each member of structure γ_i ($i = 1, 2, \ldots, 9$)), geometric parameters (e.g. the slab thickness of main girder K_a, the area coefficient of cable K_b, and the section

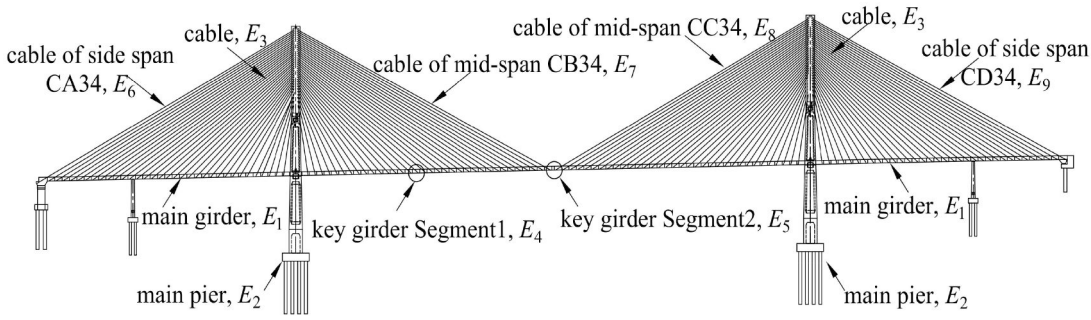

Figure 7. Annotations for the material elastic modulus in the cable-stayed bridge.

Table 3. Damage conditions (DC).

DC	Elastic modulus of damaged girder segments & cables	DC	Elastic modulus of damaged girder segments & cables
DC1	E_4, E_5 & E_6, E_7, E_8, E_9	DC8	E_4, E_5 & E_6, E_9
DC2	E_4, E_5 & E_6, E_7, E_8	DC9	E_4, E_5 & E_7, E_8
DC3	E_4, E_5 & E_7, E_8, E_9	DC10	E_4 & E_6, E_9
DC4	E_4, E_5 & E_6, E_8, E_9	DC11	E_4 & E_7, E_8
DC5	E_4, E_5 & E_6, E_7, E_9	DC12	E_5 & E_6, E_9
DC6	E_4 & E_6, E_7, E_8, E_9	DC13	E_5 & E_7, E_8
DC7	E_5 & E_6, E_7, E_8, E_9		

Table 4. Calculation results of the surrogate model under DC1 (units: m).

D_{6789} \ D_{45}	0	0.1	0.2	0.3	0.4	0.5
0	0.598	0.646	0.687	0.752	0.794	0.809
0.1	0.625	0.658	0.696	0.752	0.795	0.810
0.2	0.641	0.659	0.699	0.768	0.827	0.841
0.3	0.649	0.685	0.730	0.787	0.838	0.866
0.4	0.651	0.696	0.735	0.799	0.840	0.912
0.5	0.655	0.709	0.758	0.800	0.881	0.963

Note: D_{45} denotes the damage degree of E_4 and E_5; D_{6789} denotes damage degree of E_6, E_7, E_8 and E_9.

thickness of main pier t), and load parameters (e.g. secondary load q_1 and vehicle load q_2). They are assumed to be independent, and the parameters are listed in Table A1.

4.3.3. Displacement solving for the cable-stayed bridge

In Table A1, there are 2 load variables, and 23 variables in total. The uniform design table of U_{120} (120^{23}) is generated and listed in Table A2. With the method proposed in this paper, five response surfaces are obtained, and the limit state equation is obtained after 9 iterations. The coefficients corresponding to the five response surfaces are given in Table A3, and they are employed to solve the displacements under 13 damage conditions proposed in this paper. Then, with the displacement solving method proposed in this paper, the deflections can be acquired.

The mid-span deflection of the main girder under any damage condition is calculated by sampling analysis based on the mean value of variables and the damage degree. The calculation results of the surrogate model under the most unfavorable damage condition DC1 are listed in Table 4 as an example. It can be seen that the mid-span deflection is influenced by two variables (damage degree of girders and cables). Taking the damage degree of the girders and cables as the main variable, respectively, Figure 8 is obtained. From the comparison in Figure 8, it can be seen that the mid-span deflection of the main girder gradually increases with the increase of the damage degree of the girder and the cables. Besides, this trend is also applicable to other damage conditions.

To verify the accuracy of the surrogate model, it is necessary to calculate the calculation error between the surrogate model and the finite element model. Let Δ_{S1} denote the deflection of the cable-stayed bridge calculated by the surrogate model, Δ_{S2} denote the deflection calculated by the finite element model. Then, the errors between the deflections acquired by the surrogate model and finite element model, respectively, can be calculated as:

$$Error = \frac{|\Delta_{S1} - \Delta_{S2}|}{\Delta_{S2}} \times 100\% \tag{26}$$

Taking the most unfavorable condition DC1 as an example, the errors are listed in Table 5. From Table 5, it can be seen that the maximum error of the mid-span deflection calculated by the surrogate model and ANSYS is about 12%, while the minimum error of that is about 1%. In addition, the calculation error under other damage conditions is also not large. This indicates that the surrogate model fitted based on the MRS method can be well applied in calculating the mid-span deflection of the long-span bridges, and the coefficient of the surrogate model is applicable to the displacement solving under any damage conditions for this engineering example.

4.3.4. Uncertainty analysis of structural displacement

Based on the surrogate model for solving structural displacement in Section 4.3.3, MCS is employed to obtain the uncertainty parameters of mid-span deflection (e.g. the mean value and the coefficient of variation) under any damage conditions in the MATLAB computing environment. Firstly, at different service years, the time-related random variables in Table A1 need to select the corresponding uncertainty parameters according to the service moment t for sampling analysis, while the other variables in Table A1 select the same uncertainty parameters. Subsequently, the random samples are taken into the displacement solving model proposed in this study to obtain the corresponding deflections. Finally, the structural displacements under different damage conditions and service years are statistically analyzed, respectively.

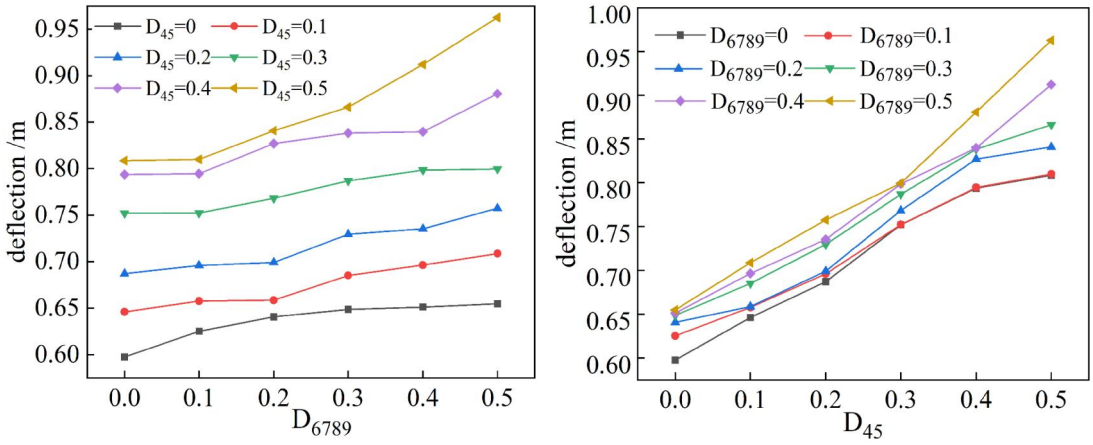

Figure 8. Diagram for the mid-span deflection under different damage types.

Table 5. Error in mid-span deflection of main girder for DC1.

D_{6789} \ D_{45}	0	0.1	0.2	0.3	0.4	0.5
0	5.57%	4.20%	4.16%	1.09%	1.36%	3.64%
0.1	1.20%	2.49%	2.93%	1.08%	1.30%	4.22%
0.2	1.26 %	2.36%	2.51%	0.98%	2.69%	1.19%
0.3	2.52%	1.56%	1.69%	3.38%	4.02%	1.70%
0.4	2.93%	3.20%	2.47%	4.84%	4.11%	6.98%
0.5	3.48%	4.99%	5.49%	4.89%	9.07%	12.74%

Note: D_{45} denotes the damage degree of E_4 and E_5; D_{6789} denotes damage degree of E_6, E_7, E_8 and E_9.

Table 6. Uncertainty parameters of deflection when $t = 30$a.

Condition	μ /m	*cov*	Condition	μ /m	*cov*
DC0	0.728	0.248	DC7	0.712	0.278
DC1	0.780	0.240	DC8	0.724	0.231
DC2	0.766	0.208	DC9	0.751	0.200
DC3	0.743	0.259	DC10	0.722	0.243
DC4	0.706	0.240	DC11	0.739	0.266
DC5	0.724	0.259	DC12	0.730	0.287
DC6	0.701	0.236	DC13	0.767	0.249

Note: DC0 denotes the initial state of the bridge (when $t = 0$), and there is no damage.

The corresponding statistical parameters of mid-span deflection under different damage conditions and service years are listed in Tables 6 and 7. Compared to the new construction time, the statistical parameters of main girder deflection have different degrees of variation under various damage conditions at 30a and 50a. In addition, regardless of any damage conditions, the mean value of mid-span deflection of the cable-stayed bridge generally shows an increasing trend, while the variation coefficient fluctuates to different extents.

4.3.5. Sensitivity analysis of the structural displacement

It is known that sensitivity analysis is also an important tool for uncertainty quantification, and it can evaluate the contribution of each uncertain factor to the variability of structural response in the case of multiple influence factors. Moreover, the Sobol method is a widely used tool for global sensitivity analysis with variance decomposition (Xu, Wang, Xia, Zhu, & Chen, 2023). It can calculate the contribution of the variance of a single input variable or a set of input variables to the output variance by decomposing the model

Table 7. Uncertainty parameters of deflection when $t = 50$a.

Condition	μ /m	*cov*	Condition	μ /m	*cov*
DC0	0.728	0.248	DC7	0.788	0.271
DC1	0.774	0.211	DC8	0.738	0.223
DC2	0.776	0.232	DC9	0.755	0.260
DC3	0.785	0.232	DC10	0.720	0.238
DC4	0.742	0.293	DC11	0.744	0.216
DC5	0.747	0.261	DC12	0.737	0.276
DC6	0.773	0.206	DC13	0.766	0.287

into a function of single variable and its combination. The specific are as follows.

1. Suppose the objective function is $Y = f(\boldsymbol{X})$, where $\boldsymbol{X}$ is a vector of v random variables $(x_1, x_2, \ldots, x_v)$.
2. With the Monte Carlo sampling method, two different sample matrices ($\boldsymbol{G}_{w\times v}$ and $\boldsymbol{H}_{w\times v}$) are produced by running w times respectively based on the uncertainty parameters of v random variables, where $\boldsymbol{G} = [G_1, G_2, \ldots, G_v]$; $\boldsymbol{H} = [H_1, H_2, \ldots, H_v]$. Let $\boldsymbol{H}_i$ replace $\boldsymbol{G}_i$ $(i = 1, 2, \ldots, v)$, afterwards, a new sample matrix $\boldsymbol{G}_{\boldsymbol{Hi}} = [G_1, \ldots, H_i, \ldots, G_v]$ is acquired.
3. Three groups of output results are calculated for each sample in the matrices $\boldsymbol{G}$, $\boldsymbol{H}$, and $\boldsymbol{G}_{\boldsymbol{Hi}}$ $(i = 1, 2, \ldots, v)$, and they are namely $Y(\boldsymbol{G})$, $Y(\boldsymbol{H})$, and $Y(\boldsymbol{G}_{\boldsymbol{Hi}})$, respectively.
4. The main sensitivity indices S_i and total sensitivity indices S_{Ti} are calculated as:

$$S_i = \frac{\mathrm{var}\left(E_{\boldsymbol{x}_{\sim i}}(Y|x_i)\right)}{\mathrm{var}(Y)} \tag{27}$$

$$S_{Ti} = \frac{E_{\boldsymbol{x}_{\sim i}}\left(\mathrm{var}_{x_i}(Y|\boldsymbol{x}_{\sim i})\right)}{\mathrm{var}(Y)} \tag{28}$$

$$\mathrm{var}\left(E_{\boldsymbol{x}_{\sim i}}(Y|x_i)\right) \approx \frac{1}{w}\sum_{j=1}^{w} Y(\boldsymbol{H})_j\left[Y(\boldsymbol{G}_{\boldsymbol{Hi}})_j - Y(\boldsymbol{H})_j\right] \tag{29}$$

$$E_{\boldsymbol{x}_{\sim i}}\left(\mathrm{var}_{x_i}(Y|\boldsymbol{x}_{\sim i})\right) \approx \frac{1}{2w}\sum_{j=1}^{w}\left[Y(\boldsymbol{G})_j - Y(\boldsymbol{G}_{\boldsymbol{Hi}})_j\right]^2 \tag{30}$$

where S_i reflects the contribution to the output variance caused by the individual change of variable x_i;$\mathrm{var}(Y) = \mathrm{var}(Y(\boldsymbol{G}), Y(\boldsymbol{H}))$;$S_{Ti}$ reflects the contribution of

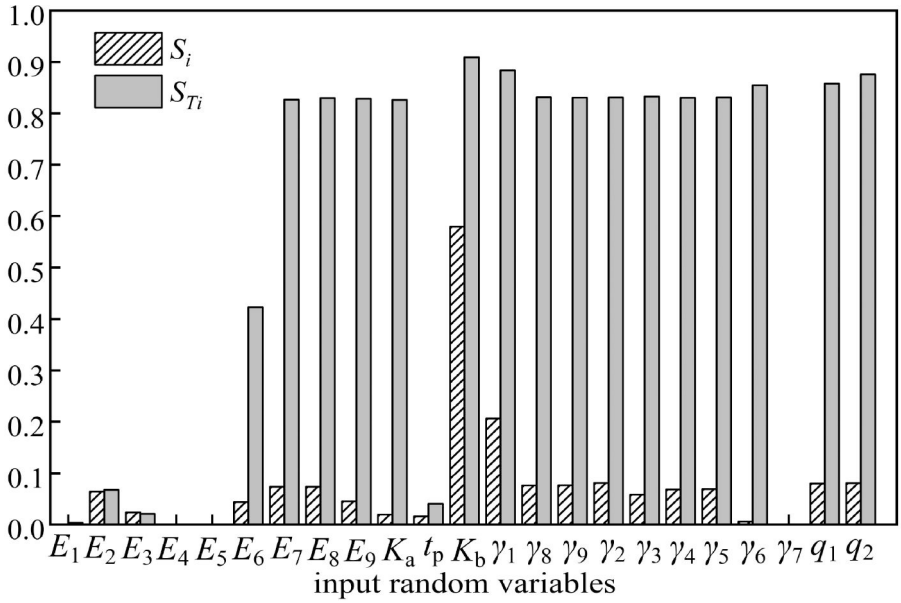

Figure 9. Sensitivity indices of structural displacement Δ_S when $t = 50$a.

Table 8. Uncertainty parameters of damaged index at different service time.

	$t = 0$a		$t = 30$a		$t = 50$a	
Variable	μ	cov	μ	cov	μ	cov
Elastic modulus of concrete E_C /Pa	3.64×10^{10}	0.100	3.32×10^{10}	0.114	3.13×10^{10}	0.123
Elastic modulus of cable E_S /Pa	1.95×10^{11}	0.100	1.69×10^{11}	0.119	1.53×10^{11}	0.130
Stiffness of girder section K /N·m^2	9.24×10^{11}	0.103	8.08×10^{11}	0.106	7.84×10^{11}	0.110
Deflection of main girder Δ_S /m	0.728	0.248	0.761	0.248	0.770	0.250

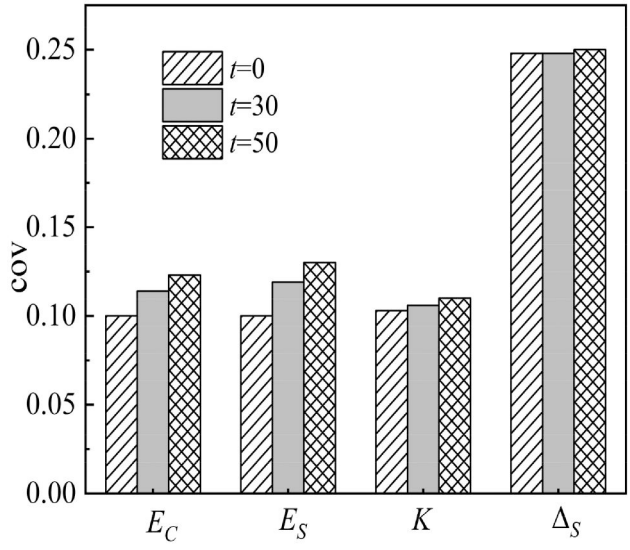

Figure 10. Variation coefficient of damage indexes of cable-stayed bridge at different service time.

variable x_i to the output variance, including all arbitrary-order variances caused by interactions with other variables $\boldsymbol{x}_{\sim i} = (x_1, \ldots, x_{i-1}, x_{i+1}, \ldots, x_v)$.

The most unfavorable damage condition DC1 is selected as an example to calculate the sensitivity indices. According to the engineering example, there are 23 input random variables, with 20000 Monte Carlo sampling, the random samples are produced based on the parameters in Table A1. Next, with the structural displacement surrogate model proposed in this paper, the corresponding structural displacements are acquired. Afterwards, the sensitivity indices can be calculated with Equation (27) and Equation (28). The results are drawn in Figure 9.

From the comparison of main sensitivity indices S_i, it can be seen that the area coefficient of cable K_b and the gravity of main girder γ_1 contribute more to the variance of the structural displacement, while the sensitivity indices of other input variables are relatively smaller. This indicates that the variance of the structural displacement will change greater when the single variable K_b or γ_1 changes. Moreover, the results of total sensitivity indices S_{Ti} show that the interaction among random variables also has a great influence on the variance of the structural displacement, and the interaction between γ_6 and other variables is more obvious. In addition, it should be also noted that the results (Figure 9) are only applicable for the surrogate model and variables in this study, and there may be different results in other structures.

4.4. Discussion of the uncertainty analysis results of structural displacement with damages

The calculation results of structural displacement under 13 damage conditions were collected and subjected to statistical analysis, then, the uncertainty parameters of the mid-span deflection under the corresponding service time are obtained. With Monte Carlo method, the uncertainty parameters of the damage indexes of materials, section of

members are quantified for the cable-stayed bridge at different service years. The details are listed in Table 8 and Figure 10.

From the comparison in Figure 10, it can be seen that the uncertainty of the structural displacement is more important than that of the material elastic modulus or the stiffness of the girder section under any service time. The reason may be that the uncertainty of damaged material is propagated to the structural displacement, and the complex force transmission path caused by large numbers of members also makes the propagation of uncertainty have multiple possibilities. However, the variation coefficient of the stiffness of the main girder is lower than that of the material elastic modulus. The reason may be that the main girder section is divided into damaged and undamaged parts in the damage mode of the members, and the variability mainly comes from the damaged concrete.

5. Conclusions

This study proposed a surrogate model to solve the structural displacement based on the multi-response surfaces method for a long-span cable-stayed bridge with damages. In this surrogate model, the uncertain damages are considered from three parts: materials, members, and structures. Taking 13 damage conditions as examples, the corresponding displacements were solved with the surrogate model, and the uncertainty parameters of structural displacement were obtained. In addition, the contribution of single random variable to the variability of displacement was quantified with the sensitivity analysis. The main conclusions that can be drawn are as follows:

1. An efficient structural displacement-solving model with dozens of variables (e.g. 23 variables) can be built based on the multi-response surfaces method for the structure with linear mechanical behavior under the normal use condition. Moreover, the proposed model can achieve an accurate approximation and can be well applied to long-span structures.
2. Based on the proposed efficient displacement-solving model, the time-varying damaged material elastic modulus and the structural damage mode can be considered easily, and the uncertainty parameters of structural displacement can be obtained quickly and practically for the long-span cable-stayed bridge.
3. With the Sobol method, the contribution of each variable to the variability of structural displacement under the most unfavorable damage condition is quantified. For the contribution of a single variable, the area coefficient of the cable or the gravity of the main girder contributes more to the variance of the structural displacement than other random variables.
4. The uncertainty of displacement under various damage conditions is quantified with MCS, and the variation coefficient of structural displacement is about twice that of the damaged material elastic modulus or the stiffness of damaged girder sections. This may because the uncertainty of displacement is influenced by variability in the loads and structural damage mode besides the damaged material.

This study shows that the multi-response surfaces method can be well applied to solve structural displacement of long-span bridges. The sensitivity analysis can quantify the contribution of each factor to the displacement and identify the uncertain factors that should be paid special attention. However, the dynamic effects of bridge structure caused by autocorrelation of the loads are neglected. Moreover, the surrogate model only studies the cases of linear elastic structural behavior under the normal use condition. Therefore, further studies are needed to consider the dynamic effects caused by autocorrelation of the loads in uncertainty quantification and to solve the structural displacement of long-span structures with the nonlinear structural behavior.

Acknowledgements

The research is supported by the National Key R&D Program of China (Grant No. 2021YFB2600900), the National Natural Science Foundation Program of China (Grant Nos.: 52378126 and 52408154), and the Provincial Natural Science Foundation of Hunan, China (Grant Nos.: 2022JJ10050 and 2023JJ40036).

Disclosure statement

No potential conflict of interest was reported by the author(s).

Data availability statement

All data, models, and code generated or used in the study can obtain from the authors.

References

Al-Mosawe, D., Neves, L., & Owen, J. (2022). Reliability analysis of deteriorated post-tensioned concrete bridges: The case study of Ynys-y-Gwas bridge in UK. *Structures*, *41*, 242–259. doi:10.1016/j.istruc.2022.04.094

Bian, H., Liu, Y., Guo, Y., Liu, Y., & Shi, W. (2023). Investigating stress-strain relationship and damage constitutive model of basalt fiber reinforced concrete under uniaxial compression. *Journal of Building Engineering*, *73*, 106789. doi:10.1016/j.jobe.2023.106789

Campione, G., & Zizzo, M. (2022). Influence of strands corrosion on the flexural behavior of prestressed concrete beams. *Structures*, *45*, 1366–1375. doi:10.1016/j.istruc.2022.09.073

Chen, A., Zhang, P., Chen, B., Li, Y., & Xing, J. (2023). A new ductile fracture model for Q460C high-strength structural steel under monotonic loading: Experimental and numerical investigation. *Engineering Fracture Mechanics*, *288*(4), 109358. doi:10.1016/j.engfracmech.2023.109358

Elsalamawy, M., Mohamed, A. R., & Kamal, E. M. (2019). The role of relative humidity and cement type on carbonation resistance of concrete. *Alexandria Engineering Journal*, *58*(4), 1257–1264. doi:10.1016/j.aej.2019.10.008

Fang, K., Lin, D., Winker, P., & Zhang, Y. (2000). Uniform design: Theory and application. *Technometrics*, *42*(3), 237–248. doi:10.1080/00401706.2000.10486045

Hadidi, A., Azar, B. F., & Rafiee, A. (2017). Efficient response surface method for high-dimensional structural reliability analysis. *Structural Safety*, *68*, 15–27. doi:10.1016/j.strusafe.2017.03.006

Hoang, V., Kiyomiya, O., & An, T. (2018). Experimental and numerical study of lateral cable rupture in cable-stayed bridges: Case study. *Journal of Bridge Engineering*, *23*(6), 05018004. BE. 1943-5592.0001227 doi:10.1061/(ASCE)

Jiang, Y., Huang, X., Liao, G., & Zhang, J. (2015a). Stable fitting of complex failure functions and correct classifying of sample points based on multiple linear support vector machines. [In Chinese] *Chinese Journal of Computional Mechanics*, *32*(03), 313–321. doi:10.7511/jslx201503004

Jiang, Y., Luo, J., Liao, G., Zhao, Y., & Zhang, J. (2015b). An efficient method for generation of uniform support vector and its application in structural failure function fitting. *Structural Safety*, *54*, 1–9. doi:10.1016/j.strusafe.2014.12.004

Jiang, Y., Zhang, X., Beer, M., Zhou, H., & Leng, Y. (2024). An efficient method for reliability-based design optimization of structures under random excitation by mapping between reliability and operator norm. *Reliability Engineering & System Safety*, *245*, 109972. doi:10.1016/j.ress.2024.109972

Jiang, Y., Zhao, L., Beer, M., Patelli, E., Broggi, M., Luo, J., … Zhang, J. (2017). Multiple response surfaces method with advanced classification of samples for structural failure function fitting. *Structural Safety*, *64*, 87–97. doi:10.1016/j.strusafe.2016.10.002

Jiang, Y., Zhao, L., Beer, M., Wang, L., & Zhang, J. (2020). Dominant failure mode analysis using representative samples obtained by multiple response surfaces method. *Probabilistic Engineering Mechanics*, *59*(1), 103005. doi:10.1016/j.probengmech.2019.103005

Jiang, Y., Zhou, H., Wang, L., Chen, Z., Tang, T., & Adhikari, S. (2021). Reliability evaluation based on Multiple Response Surfaces method considering construction uncertainties of cable tension for a hybrid roof structure. *ASCE-ASME Journal of Risk and Uncertainty Engineering Systems Part A.-Civil Engineering*, *7*(3), 04021033. doi:10.1061/AJRUA6.0001152

Ju, S., Shenoi, R. A., Jiang, D., & Sobey, A. J. (2013). Multi-parameter optimization of lightweight composite triangular truss structure based on response surface methodology. *Composite Structures*, *97*, 107–116. doi:10.1016/j.compstruct.2012.10.025

Kachanov, L. M. (1999). Rupture time under creep conditions. *Intrenational Journal of Fracture*, *97*(1), 11–18. doi:10.1023/A:1018671022008

Lemaitre, J. (1971). *Evalution of dissipation and damage in metals submitted to dynamic loading*. Proceedings of International Conference of Mechanical Behavior of Materials 1st, Kyoto, Japan.

Liu, M., Ju, X., Wu, L., Guo, Q., Wang, H., & Zhang, W. (2023). Carbonation depth model for loaded reinforced concrete (RC) beams under time-dependent relative humidity conditions. *Journal of Building Engineering*, *65*(4), 105618. doi:10.1016/j.jobe.2022.105618

Londhe, S. N., Kulkarni, P. S., Dixit, P. R., Silva, A., Neves, R., & de Brito, J. (2021). Predicting carbonation coefficient using artificial neural networks and genetic programming. *Journal of Building Engineering*, *39*(8), 102258. doi:10.1016/j.jobe.2021.102258

Lu, D., Meng, F., Zhou, X., Wang, G., & Du, X. (2022). Double scalar variables plastic-damage model for concrete. *Journal of Engineerng Mechanics*, *148*(2), 04021143. doi:10.1061/(ASCE)EM.1943-7889.0002050

Lu, Z., Zhou, Q., Li, H., & Zhao, Y. (2021). A new empirical model for residual flexural capacity of corroded post-tensioned prestressed concrete beams. *Structures*, *34*(9), 4308–4321. doi:10.1016/j.istruc.2021.10.005

Lubliner, J., Oliver, J., Oller, S., & Oñate, E. (1989). A plastic-damage model for concrete. *International Journal of Solids and Structures*, *25*(3), 299–326. doi:10.1016/0020-7683(89)90050-4

Ma, Y., Peng, A., Lei, W., & Zhang, J. (2022). Model test on static performance degradation of cable-stayed bridge with cable rupture and main girder damage. *Journal of Central South University (Science and Technology)*, *53*(02), 653–664. doi:10.11817/j.issn.1672-7207.2022.02.028

Margolin, B., Fomenko, V., Shvetsova, V., & Yurchenko, E. (2022). On the link of the embrittlement mechanisms and microcrack nucleation and propagation properties for RPV steels. Part I. Materials, study strategy and deformation properties. *Engineering Fracture Mechanics*, *267*(11), 108400. doi:10.1016/j.engfracmech.2022.108400

Meda, A., Mostosi, S., Rinaldi, Z., & Riva, P. (2014). Experimental evaluation of the corrosion influence on the cyclic behaviour of RC columns. *Engineering Structures*, *76*, 112–123. 2014.06.043 doi:10.1016/j.engstruct

Ministry of Communications and Transportation. (2020). *Specifications for design of highway cable-stayed bridge*. JTG/T3365-01-2020. Beijing, China: China Communications Press.

Mourlas, C., Markou, G., & Papadrakakis, M. (2019). Accurate and computationally efficient nonlinear static and dynamic analysis of reinforced concrete structures considering damage factors. *Engineering Structures*, *178*, 258–285. doi:10.1016/j.engstruct.2018.10.034

Nazarian, E., Ansari, F., Zhang, X., & Taylor, T. (2016). Detection of tension loss in cables of cable-stayed bridges by distributed monitoring of bridge deck strains. *Journal of Structural Engineering*, *142*(6), 04016018. doi:10.1061/(ASCE)ST.1943-541X.0001463

Paul, S. C., Panda, B., Huang, Y., Garg, A., & Peng, X. (2018). An empirical model design for evaluation and estimation of carbonation depth in concrete. *Measurement*, *124*, 205–210. doi:10.1016/j.measurement.2018.04.033

Rabotnov, Y. N. (1963). Paper 68: On the equation of state of creep. *Proceedings of the Institution of Mechanical Engineers*, *178*(1), 2-117–2-122. doi:10.1243/PIME_CONF_1963_178_030_02

Ren, W., Fang, S., & Deng, M. (2011). Response surface-based finite-element-model updating using structural static responses. *Journal of Engineering Mechanics*, *137*(4), 248–257. doi:10.1061/(ASCE)EM.1943-7889.0000223

Shang, M., Yang, H., Su, A., & Wang, Y. (2023). Strain-rate and stress-state dependent ductile fracture model of S690 high-strength steel. *Journal of Constructional Steel Research*, *204*, 107852. 2023. 107852 doi:10.1016/j.jcsr

Shen, Z., & Wu, A. (2007). Seismic analysis of steel structures considering damage cumulation. *Frontiers of Architecture and Civil Engineering in China*, *1*(1), 1–11. doi:10.1007/s11709-007-0001-7

Truong, V., & Kim, S. (2017). An efficient method of system reliability analysis of steel cable-stayed bridges. *Advances in Engineering Software*, *114*, 295–311. 07.011 doi:10.1016/j.advengsoft.2017

Wang, D., & Tang, H. (2014). The static system reliability of cable-stayed bridges using the response surface method. *Journal of Transport Science and Engineering*, *30*(02), 34–39. doi:10.3969/j.issn.1674-599X.2014.02.006

Wang, P., Zhang, L., Wang, F., & Zhang, Z. (2015). Research on influences of time-varying effect of steel strand corrosion on pressurised concrete beam bridges. *Technology of Highway and Transport*, *31*(01), 66–72 + 82. doi:10.13607/j.cnki.gljt.2015.01.0014

Wang, Y. (2023). A 3D stochastic damage model for concrete under monotonic and cyclic loadings. *Cement and Concrete Research*, *171*, 107208. doi:10.1016/j.cemconres.2023.107208

Wang, Y., & Li, J. (2022). Stochastic fatigue damage model for concrete under complex stress states. *Science China Technological Sciences*, *65*(11), 2641–2648. doi:10.1007/s11431-021-2070-5

Wang, Y., Liao, T., Chi, H., Lai, Z., Qin, J., & Huang, R. (2023). Damage behavior of concrete members subjected to underwater contact explosion. *Engineering Failure Analysis*, *151*, 107412. doi:10.1016/j.engfailanal.2023.107412

Wei, X., & Pan, Z. (2020). Study on the influence of cable damage at different positions on the mechanical properties of cable-stayed bridges. *Gansu Science and Technology*, *36*(04), 91–94. doi:10.3969/j.issn.1000-0952.2020.04.029

Xu, B., Wang, S., Xia, H., Zhu, Z., & Chen, X. (2023). A global sensitivity analysis method for safety influencing factors of RCC dams based on ISSA-ELM-Sobol. *Structures*, *51*, 288–302. doi:10.1016/j.istruc.2023.03.027

Yan, R., Wen, Q., Wang, S., Sun, T., Liu, H., & Zhang, P. (2023). Study on cable property degradation under accelerated corrosion test. *China Civil Engineering Journal*, *56*(05), 18–31. doi:10.15951/j.tmgcxb.21121224

Yu, Q., Gu, X., Zeng, Y., & Zhang, W. (2022). Flexural behavior of corrosion-damaged prestressed concrete beams. *Engineering Structures*, *272*, 114985. doi:10.1016/j.engstruct.2022.114985

Zhang, Y., Fang, Z., Jiang, R., Xiang, Y., Long, H., & Lu, J. (2020). Static performance of a long-span concrete cable-stayed bridge subjected to multiple-cable loss during construction. *Journal of Bridge Engineering*, *25*(3), 04020002. doi:10.1061/(ASCE)BE.1943-5592.0001529

Zhang, Y., Lu, Z., & Cao, Y. (2020). Unified strength model based on the Hoek-Brown failure criterion for fibre-reinforced polymer-confined pre-damaged concrete columns with circular and square cross sections. *Journal of Central South University*, *27*(12), 3807–3820. doi:10.1007/s11771-020-4563-z

Zhang, Z., Li, W., Ding, Z., & Wu, X. (2020). An approach to the selection of target reliability index of cable-stayed bridge's main girder based on optimal structural parameter ratio from cost-benefit analysis. *Structures*, *28*, 2221–2231. doi:10.1016/j.istruc.2020.10.046

Zheng, Y., & Wang, Y. (2018). Research on seismic performance of long-span steel bridge considering time-dependent damage characteristics. *Modern Transportation Technology*, *15*(02), 30–37. doi:10.3969/j.issn.1672-9889.2018.02.008